The design and performance of a smart ball-and-socket actuator

El-Wahed, Ali; Balkhoyor, Loaie; Wang, Haochen

Published in:
International Journal of Applied Electromagnetics and Mechanics

DOI:
10.3233/JAE-170039

Publication date:
2019

Document Version
Peer reviewed version

The Design and Performance of a Smart Ball-and-Socket Actuator

Ali K. El Wahed*, Loaie B. Balkhoyor and HaoChen Wang

Mechanical Engineering, University of Dundee, Dundee DD2 5LG, U.K.

**Corresponding author, email: a.elwahed@dundee.ac.uk; Tel.: 0044 1382384496*

Abstract.

In this paper, the design and performance of a multi-degree-of-freedom smart ball-and-socket actuator and its application to rehabilitation training systems are investigated. A key feature of this actuator is the use of magnetorheological fluids which can exhibit dramatic changes in their rheological properties, including yield stress, when subjected to external magnetic fields. These fast and reversible fluid rheological changes permit the smart actuator to provide the required impedance at orthotic arm joints aimed for upper-limb rehabilitation.

Electromagnetic finite element analyses using ANSYS software were carried out to design the electromagnetic circuit of the actuator and important design factors affecting the efficiency of the generated magnetic field and its best delivery to the MR fluid, were examined. These factors included the relative permeability of the magnetic material and the electromagnetic coil properties such as its shape, size and location. In addition, the utilisation of non-magnetic materials in the electromagnetic circuit design was investigated with the aim to optimise the performance of the smart actuator.

Finally, the performance of the smart actuator was assessed theoretically and numerically under various input conditions in which Bingham plastic fluid characteristics were assumed, and the results determined by the two techniques were found to compare well.

Keywords: Magnetorheological Fluids, Electromagnetic Design, Ball-and-Socket Actuator

1. Introduction

It is estimated that 10% of the total world population is disabled. This equates to approximately 600 million disabled people. Critical to this group of people would be the fact that the population of old people (aged 65 years and older) will reach a total of approximately 800 million by 2025 [1]. There are several reasons that lead to disabilities. Stroke is a leading cause, particularly affecting older people, with an estimated annual incidence of 180, 125, 200 and 280 people per 100,000 citizens in the USA, Europe, England and Scotland, respectively [2]. Statistics from England and Wales show that every year approximately 100,000 people experience a stroke for the first time, out of which 10,000 are under the retirement age. Approximately one-third of the people surviving a stroke are left with severe disabilities [3]. Moreover, it has been noticed that due to the rapid aging of the society in recent times, the number of people with limb disabilities has been increasing [4].

Muscle strengthening with resistance training has been reported to have positive effects on the recovery of normal physiological functions after neurological or traumatic injuries. A number of studies have shown that resistance training results in improved mobility, reduced pain and better stability [5]. Rehabilitation devices have been invented and introduced for use in the healthcare sector in order to reduce the cost of the rehabilitation care and to substitute for the current shortage in the number of the experienced physiotherapists.

The need for light-weight rehabilitation devices with improved performance (yet resilient enough to execute the exercises), which can be adjusted according to the requirements of the muscle strengthening and the resistance training protocols has led to the utilisation of smart materials such as magnetorheological (MR) [6-8] and electrorheological (ER) [9-11] fluids. MR and ER fluids are smart suspensions, whose rheological properties can be quickly tuned by an external magnetic or electric field, respectively. A very important feature of the MR/ER fluids is the reversibility of their rheological phase, which usually happens within milliseconds

[12]. MR fluids consist of fine ferromagnetic particles suspended in a non-magnetic carrier fluid. They exhibit a controllable shear yield stress under controllable external magnetic fields. The particles are usually 1-10 μm in diameter.

This paper summarises the work carried out by the authors on the design and performance evaluation of a smart ball-and-socket actuator that utilises MR fluids to control its output. This is accomplished by changing the yield strength of the MR fluid in accordance to an externally applied magnetic field which is supplied by a toroidally-shaped electromagnetic coil element. Early work on this project was carried out by the authors in 2009 when the results validated the required design specifications [13]. The developed actuator with its multi-degrees-of-freedom capability is designed to enhance the function of upper-limb rehabilitation training systems, which should help patients to regain independence by relearning the lost skills and functions of their upper extremities. The application of a spherical brake for haptics was reported earlier [14]. Also, recent attempts have suggested the use of an electrorheological spherical actuator for applications in robot-assisted cutting surgery [15].

2. The Ball-and-Socket Actuator Concept

The aim of this study is to design smart a ball-and-socket actuator which could be incorporated into the joints of an orthotic device that is aimed for the rehabilitation of patients with upper-limb impairments. Clearly, this orthosis requires three flexible joints which are located at the shoulder, elbow and wrist levels. Accordingly, three smart actuators should be added to these three joints to provide the variable impedance requirement. These impedances are expected to vary from large values at the shoulder joint to smaller values at the elbow and wrist joints. The main advantage of the ball-and-socket joint is that it has the capability to provide multi-degree-of-freedom (MDOF) motions. The conceptual design of the smart ball-and-socket actuator is shown in Fig 1 (a). It is considered as a perfect match for human upper-limb joints, as shown in Fig. 1(b).

The work reported in this paper is focused on the development of a smart ball-and-socket actuator for the shoulder joint only. The human shoulder is capable of providing flexion/extension torques with a peak value of about 110 N.m as well as adduction/abduction torques with a peak value of about 125 N.m [16]. However shoulder rehabilitation orthoses are usually designed with a torque capability that is well below these peak values, which is normally set at 50 N.m [17]. This is because the output torque is not constant for the whole range of motions and its peak value is only required at specific joint positions [18]. In order to meet the required shoulder movements, the proposed ball-and-socket joint has been designed with an opening angle (from one socket edge to another) of 125°.

The efficient excitation of MR fluids requires a magnetic circuit that consists of a source of magnetic flux (current-carrying coils) and a path to deliver it to the fluid. The dynamic yield stress of the MR fluid is altered depending on the magnetic field intensity [19]. An optimum design of the magnetic circuit is necessary to produce a light-weight electromagnetic device that is capable of delivering the required magnetic field with the minimum electrical power consumption. Furthermore, in order to ensure a consistent performance of the MR device, the electromagnetic element should generate a uniformly distributed magnetic field across the majority of the MR fluid volume. In this work, the magnetic flux uniformity is assessed and monitored along an imaginary trajectory path passing through the middle part of the MR fluid gap between the socket and the ball components of the smart actuator. The target would be to achieve a uniform flux density distribution in the range of 1.3–1.5 Tesla along this predefined path, which represents the saturation point for most commercial MR fluids [20].

The electromagnetic analyses of the ball-and-socket actuator are carried out using ANSYS finite element analysis software, which is a general-purpose modelling package for solving a wide range of engineering problems including structural, heat transfer and computational fluid dynamics (CFD), acoustic, and electromagnetic.

3. Actuator Design Parameters

In order to optimise the function of the ball-and-socket actuator, all possible design-influencing parameters were systematically determined. The critical design parameters that affect the operation of the smart actuator were identified and listed below:

1- Size of the actuator ball.

2- MR fluid gap size.

3- MR fluid properties.

4- Magnetic properties of the ball and socket materials.

5- Electromagnetic coil characteristics.

6- Non-magnetic material inserts and their characteristics, and

7- Overall geometry of the actuator.

The first three parameters in the above list are discussed in this section. They were determined following both analytical and logical approaches. The rest of the design parameters were analyzed and their optimum values were determined, which will be detailed in Section 4 of this manuscript.

To calculate the size of the actuator ball, the Bingham plastic fluid model was utilized in this process. This is the most commonly used non-Newtonian fluid model [21] to describe the characteristics of MR fluids, which are governed by the following equation:

$$\tau = \eta\,\gamma + \tau_y\left(H\right) \qquad (1)$$

where τ, $\tau_y(H)$ and η are the shear stress, dynamic yield stress which is dependent on the magnetic field intensity, H, and the dynamic viscosity of the MR fluid, respectively whilst γ is the shear rate. The total torque T_t delivered by the MR ball-and-socket joint comprises three components. These are the controllable field-dependent torque T_y, the viscous-friction torque T_v and the mechanical-friction torque T_m [22]. Hence, T_t is:

$$T_t = T_y + T_v + T_m \qquad (2)$$

In practical applications, the torque due to the mechanical-friction T_m, which is mainly caused by mechanical seals rubbing against the ball of the actuator, is relatively small in comparison with the other two torque components and hence, it could be discarded from the current analysis. Although, the majority of the actuator torque comes from the yield stress of the fluid, the torque due to viscous-friction T_v has been included in this analysis so that the effect of the angular velocity at which the device is utilized as part of the current rehabilitation application is also accommodated.

Since spherical components are involved in this analysis, the Cartesian *x* and *y* axes are identical and therefore, the spherical coordinate system which is shown in Fig. 2 is employed to mathematically derive the torque produced by the smart device.

The field-dependent torque T_y is first calculated by integrating a miniature torque, which is due to a shear force created by the fluid shear stress acting on an infinitesimally small area *dA* of the actuator ball, over the ball area, *A* that is in contact with the MR fluid:

$$T_y = \iint_A \tau_y(H)\, r_m \, dA \qquad (3)$$

where r_m is the moment arm, Fig. 2, that is given by:

$$r_m = r \sin\varphi \qquad (4)$$

The infinitesimal area *dA* is given by:

$$dA = r^2 \sin\varphi \, d\varphi \, d\theta \qquad (5)$$

Combining equations (3), (4) and (5) yields:

$$T_y = \int_0^{\varphi} \int_0^{2\pi} \tau_y(H)\, r \sin\varphi \, r^2 \sin\varphi \, d\varphi \, d\theta$$

$$\therefore \quad T_y = \tau_y(H)\, r^3 \int_0^{\varphi} \int_0^{2\pi} \sin^2\varphi \, d\varphi \, d\theta \qquad (6)$$

The viscous-friction T_v could also be derived following the same philosophy:

$$T_v = \iint_A \eta \, \gamma \, r_m \, dA \qquad (7)$$

The shear rate γ is given as:

$$\gamma = \frac{r_m \, \omega}{h} \qquad (8)$$

where ω is the angular velocity and h is the MR fluid gap size.

Using equation (8) and noting that the moment arm r_m and the infinitesimal area dA are still given by equations (4) and (5) respectively, equation (7) is rewritten as:

$$T_v = \int_0^{\varphi} \int_0^{2\pi} \eta \, \frac{r_m \, \omega}{h} \, r \sin\varphi \, r^2 \sin\varphi \, d\varphi \, d\theta$$

which is simplified to yield equation (9) below:

$$T_v = \int_0^{\varphi} \int_0^{2\pi} \eta \, \frac{r \sin\varphi \, \omega}{h} \, r \sin\varphi \, r^2 \sin\varphi \, d\varphi \, d\theta$$

$$T_v = \eta \, \frac{r^4 \, \omega}{h} \int_0^{\varphi} \int_0^{2\pi} \sin^3\varphi \, d\varphi \, d\theta \qquad (9)$$

Now, equations (2), (6) and (9) are combined to give the total torque T_t:

$$T_t = \tau_y(H)\, r^3 \int_0^{\varphi} \int_0^{2\pi} \sin^2\varphi \, d\varphi \, d\theta + \eta \, \frac{r^4 \, \omega}{h} \int_0^{\varphi} \int_0^{2\pi} \sin^3\varphi \, d\varphi \, d\theta \qquad (10)$$

Integration of equation (10) yields:

$$T_t = \pi \, r^3 \, \tau_y(H)\left(\varphi - \sin\varphi\cos\varphi\right) + \frac{8\,\eta\,\pi\,r^4\,\omega}{3\,h} \sin^4\left(\frac{\varphi}{2}\right)\left(\cos\varphi + 2\right) \qquad (11)$$

In order to simplify the design procedure for this application, the MR fluid gap size, h was assumed to be 2 mm. Similar fluid gap value has been successfully set in the design of various MR fluid devices (see for example [23-25]).

It was decided to employ a commercial MR fluid type Lord MRF241-ES in this investigation, which has a viscosity (at 25 °C) η = 88 mPa.s and is capable of providing yield stresses in excess of 67 kPa when energized by magnetic field intensities in excess of 200 kA/m [26]. By considering these properties of the MR fluid and also assuming a torque requirement for the shoulder joint as 50 N.m as well as an opening angle, φ (from one socket edge to another) as 125° as stated in Section 2 together with an angular velocity of 5 rad/s, equation (11) was used to determine the radius of the ball of the smart actuator, which was found to be 50 mm.

With regard to the MR fluid permeability, it was found that most commercial MR fluids that were studied have their magnetic permeabilities in the range between 3.5 and 10. This is a very narrow range which will not have a great influence on the effectiveness of the actuator's electromagnetic circuit. For the MR fluid employed in this investigation, a magnetic permeability value of 8 [26] was assumed in the assessments of the electromagnetic circuit of the smart actuator.

4. 2-D Electromagnetic Circuit Simulation

A progressive approach was adopted in order to achieve the optimum design of the ball-and-socket actuator. The methodology involves a systematic assessment the effects of the materials and dimensions of the ball-and-socket actuator components on the efficiency of the actuator's electromagnetic circuit. This includes investigating the effects of the number of electromagnetic coil elements as well as their size, location, shape and orientation on the electromagnetic circuit design. In addition, the magnetic field distribution is further optimized with the aid of a non-magnetic material inserts which are added in the magnetic path so that

the majority of the required magnetic field is directed towards the MR fluid gap only, allowing a uniform distribution of the magnetic flux density along the imaginary trajectory path. As a result, a more compact actuator design was achieved without increasing the size of the actuator. This magnetic field optimization technique was also reported in other MR fluid device designs [27].

The first major variable, which influences the quality of the magnetic field distribution in the MR fluid, is the permeability of the magnetic material. In this investigation, low carbon steel (LCS), medium permeability metals such as VimVar and MaxiMag, and high permeability metal such as MuMetal were examined. In addition, combinations of these magnetic materials for the ball and socket components were also investigated. It was found that high and medium permeability metals produced the best magnetic field distribution along the imaginary fluid path. However, the optimum electromagnetic circuit design was obtained when VimVar and MaxiMag materials were assumed for the ball and socket components of the actuator, respectively.

The second major variable that affected the distribution of the magnetic field within the MR fluid gap was the configuration of the electromagnetic coil element, which is embedded inside the socket. Various shapes, locations and sizes were investigated for the coil, with the best result elicited when the coil shape was cylindrical with a rectangular cross-section that has its top end tilted towards the outer edge of the socket.

The third major variable that influenced the results was the use of non-magnetic material inserts that are incorporated in the electromagnetic circuit to control the magnetic pathway. Again, various configurations of the non-magnetic material inserts and their locations were investigated in order to achieve the optimum uniformity of the magnetic field inside the MR fluid gap.

In order to reduce the weight of the new actuator, especially in consideration of its incorporation into an orthotic arm which is proposed for the rehabilitation of a human shoulder, the actuator's ball was designed to be hollow. Although a solid ball is expected to provide a better magnetic field distribution, the reduction in the magnetic field uniformity which is caused by using a hollow ball is overcome by optimising the configuration of the electromagnetic coil element and the non-magnetic inserts as well as their location within the socket component of the actuator. Optimisation of the ball cavity was therefore, the fourth major influencing variable that was dealt with in the development of the electromagnetic circuit of the new actuator. It was found that the best results were obtained when the inner diameter of the ball was set to 80.0 mm.

Fig. 3 shows a cross-sectional view of the smart ball-and socket actuator with the geometrical details of its optimum electromagnetic circuit whilst Fig. 4 shows a contour plot of the flux-line density in a half-section of the actuator. However, the impact of removing the non-magnetic material inserts on the magnetic flux distribution inside a half-section of the smart actuator is shown in Fig. 5. Comparing the results shown in Figs. 3 and 4, it can be seen that the non-magnetic inserts main task was to stop the short circuit path of the magnetic field within the socket part where the magnetic permeability is high and instead, it encouraged the field lines to cross the MR fluid gap and into the actuator ball where the magnetic permeability is also high.

The magnetic field density variation along half of the circular imaginary trajectory path in the middle of the MR fluid gap, starting from the lower end of to the socket opening, is illustrated in Fig. 6 for the two cases with and without the non-magnetic material inserts. The results show that the flux drops by 5%, which occurs in the fluid volume that is opposite the electromagnetic coil element (approximately around the centre part of the magnetic field path). This field drop is considered to be small in comparison with a field drop of about 80% which happens in the

absence of non-magnetic inserts, and hence it should not affect the magnetic circuit efficiency of the actuator. This issue was also encountered in previous designs of MR fluid devices (see for example [28-30]).

5. 3-D Electromagnetic Circuit Simulation

In order to confirm the results that were obtained in the 2-D simulations of the electromagnetic circuit of the ball-and-socket actuator, the optimum circuit characteristics (detailed in Section 4) were setup on the ANSYS Workbench employing the Magnetostatic module which is an add-on module used to simulate 3-D electromagnetic circuits.

The simulation was started by importing the 3-D geometry of the ball-and-socket actuator, which was created using SolidWorks CAD software, into the ANSYS Workbench environment. A step-by-step approach was employed to set up the specifications of the actuator and the electromagnetic coil. The coil located inside the socket component of the actuator consists of 488 turns of 30 AWG wire which is driven by a maximum current of 2.1 Amperes. Based on the cross sectional area of the coil, a current density of 2.277×10^7 Ampere/m^2 was estimated and subsequently input into ANSYS. The created model was then meshed (Fig. 7) and solved.

The magnetic field density values along the same imaginary median path inside the MR fluid gap were calculated, which are shown in Fig. 8. The 3-D electromagnetic simulations have shown that the maximum field density values occur in the socket part at the upper corner of the electromagnetic coil element and also at the bottom part of the non-magnetic material insert.

Fig. 9 shows a comparison between the variations of the magnetic field density along the imaginary median path inside the MR fluid gap of the actuator, which were obtained using the ANSYS 2-D and 3-D techniques. It can be seen that the data predicted using the 3-D Magnetostatic module compare well with the 2-D results. However, the fluctuations observed

in the 3-D simulation data are possibly attributed to the fact that the meshing techniques employed by the ANSYS code are different to those used by the ANSYS Workbench platform [31]. It is worth mentioning that the present 3-D Magnetostatic technique has been used to predict the performance of the electromagnetic circuit of the ball-and-socket actuator for a range of applied currents and the results are in excellent agreement with the 2-D data. This suggests that the 3-D electromagnetic simulation technique might be used as a first choice tool in the design of smart MR fluid actuators particularly when the design aspects of the device cannot be handled by straight 2-D simulations.

In the earlier work reported on the application of a spherical brake for haptics [14], only limited data were provided on the design of the electromagnetic circuit of the device whilst all important factors affecting the design process of this circuit have been thoroughly assessed in the current investigation. In addition, the actuator reported in this manuscript has been developed for the rehabilitation of human upper limbs and hence, the relevant torque and motion ranges reported in Section 2 enabled the selection of the proper dimensions and materials of the actuator and its components including the electromagnetic coil element and the magnetic path. Furthermore, the 3-D Magnetostatic analysis has confirmed the validity of the 2-D magnetic analysis particularly when the complex electromagnetic aspects of this actuator are considered.

6. Performance Evaluation of the Ball-and-Socket Actuator

The dynamic yield stress of the employed MR fluid as a function of the magnetic flux density is presented in Fig. 10. In this investigation, the MR fluid temperature was assumed to be maintained at 25 °C at which the viscosity and density of the fluid were quoted as 88 mPa.s and 3860 kg/m^3, respectively [7]. Using the yield stress magnitudes presented in Fig. 10 and equation 11, the total transmitted torques of the smart actuator were then estimated theoretically for a ball angular speed of 5 rad/s and for a range of magnetic flux densities.

Computational fluid dynamics (CFD) analyses were then performed using ANSYS CFX code to determine the performance of the smart actuator. Accordingly, a model for the MR fluid volume filling the gap between the ball and socket components was first created using SolidWorks software, which was subsequently imported into ANSYS CFX environment. Fig. 11 shows the meshed fluid volume with a minimum element size of 3.5×10^{-4} m. In these analyses, the magnetic flux density is assumed to be uniformly distributed along the fluid gap and hence, the yield stress of the MR fluid (Fig. 10) required for the CFD simulations is considered to be constant throughout the fluid volume under the same electromagnetic conditions.

The MR fluid surface which is in contact with the socket component is assumed to be stationary (no-slip condition) whilst the fluid surface in contact with the ball is considered to be moving at the ball angular speed. The top horizontal surface of the fluid at the socket opening, which is in contact with a large lip-seal that is designed to seal the fluid gap between the ball and socket components was also considered as a stationary wall.

Due to the fact that the applied angular speed is low, the MR fluid flow inside the gap initiated by the ball motion was assumed to be steady, laminar, and incompressible. Also, thermal fluid interactions were ignored and therefore, the fluid flow was considered to be under adiabatic conditions. In addition, any cavitation possibility is assumed to be remote since the minimum fluid pressure is not expected to drop below the fluid vapour pressure. The CFD solution steps are summarized in the flow chart presented in Fig. 12.

An isometric view of the fluid velocity in the gap between the ball and socket components of the actuator for magnetic excitation of 0.75 Tesla is shown in Fig.13. It can be seen that the velocity on the outer surface of the fluid volume, which is in contact with the socket surface, is zero whilst the maximum velocity is seen to occur on the fluid side that is in contact with the moving ball. Also, this velocity contour shows that the fluid velocity varies along the moving

wall, which should result into variable shear rates and corresponding shear stresses in accord with equation (1).

The CFD simulations were then completed with the estimation of the torque transmitted by the MR fluid to the socket surface in response to the ball rotation, and the results are shown in Fig. 14 for a range of the magnetic flux density. The theoretical torque results, which were estimated using equations 11, are also presented in this figure. It is clear that there is a good agreement shown between the theoretical and the CFD results. Also, both results indicate that the transmitted torque increases with the magnetic flux density before reaching a saturation point with a torque value of about 76 N.m when the fluids was excited by about 1.4 Tesla.

In general, it could be concluded that the CFD technique, which has been successfully applied in this investigation to estimate the performance of the smart ball-and-socket actuator, could be applied as a cost-effective technique to determine the performance of other smart fluid devices such as clutches, brakes, and dampers.

7. Mechanical Design of the Ball-and-Socket Actuator

The mechanical design of the ball-and-socket actuator has taken into consideration several factors including the assembly of the ball and socket components, sealing of the MR fluid inside its designated gap, winding of the coil inside the socket component, maintaining a uniform MR fluid gap (constant h along the fluid path) and insertion of the non-magnetic rings at their predesigned locations.

In order to facilitate the winding of the coil, the socket component was divided into four parts, which are fastened to each other using small screws. O-ring seals have been allowed between the socket parts in order to prevent MR fluid leakages. Also, the insertions of the two non-magnetic rings, which are manufactured from Teflon, have been taken into consideration when the four socket parts were designed. In addition, an aluminium shell was designed to encompass

the socket parts in order to prevent any electromagnetic interference with the surrounding medium. Furthermore, an opening to inject the MR fluid inside the gap between the ball and socket components was allowed at the top of the socket. Finally, in order to maintain the ball at the centre of the socket and to have a uniform MR fluid volume, five small PTFE balls were embedded in the socket component, part of which was allowed out to support the metallic ball, so that a constant fluid gap is maintained between the ball and socket parts.

8. Conclusions

In this paper, the authors have described the design process of a smart multi-degree-of-freedom (MDOF) actuator that has been proposed to assist with the rehabilitation of human upper limbs. Magnetorheological fluids were utilised to provide the controllable impedance required in the rehabilitation application of this actuator. Advanced finite element electromagnetic assessment techniques were used to design the actuator's electromagnetic circuit, which have enabled the optimum excitation of the MR fluid and also produced the most compact design of this device.

The performance of the smart actuator was determined theoretically which was verified numerically using a computational fluid dynamics (CFD) technique. The theoretical torque results, which were estimated using a model combining the viscous-friction and the controllable field-dependent characteristics of the MR fluid, agreed well with the CFD torque results. The overall device performance was found to be adequate for human upper-limb rehabilitation applications.

Acknowledgements

This research received no specific grant from any funding agency in the public, commercial or not-for-profit sectors.

References

[1] K. Shima, R. Eguchi, K. Shiba and T. Tsuji, CHRIS: cybernetic human-robot interface

systems, *International Symposium on Robotics* (Conference # 10994), 29 Nov - 01 Dec 2005, Tokyo, Japan, 1- 8.

[2] P. A. Isard and J. F. Forbes, The cost of stroke to the National-Health-Service in Scotland, *Cerebrovascular Diseases* **2** (1992), 47-50.

[3] R. Loureiro, F. Amirabdollahian, M. Topping, B. Driessen and W. Harwin, Upper limb robot mediated stroke therapy - GENTLE/s approach, *Autonomous Robots* **15** (2003), 35-51.

[4] Y. Ogura, H. Aikawa, K. Shimomura, H. Kondo, A. Morishima, H. Lim and A. Takanishiet, Development of a new humanoid robot WABIAN-2, *IEEE International Conference on Robotics and Automation*, 15-19 May 2006, Orlando, USA, 76-81.

[5] S. Dong, K. Lu, J. Sun and K. Rudolph, Smart rehabilitation devices - Part II - adaptive motion control, *Journal of Intelligent Material Systems and Structures* **17** (2006), 555-561.

[6] H. Nakano and M. Nakano, Active loading machine using MR fluid clutch for leg rehabilitation system, *International Journal of Applied Electromagnetics and Mechanics* **39** (2012), 463-469.

[7] D. Case, B. Taheri and E. Richer, Design and characterization of a small-scale magnetorheological damper for tremor suppression", *IEEE/ASME Transactions on Mechatronics* **18** (2013), 96-103.

[8] K. Miura and S. Katsura, Robust velocity constraint control of passive load system for human wearable interface, *Journal of the Japan Society for Precision Engineering* **80**(2014), 388-394.

[9] J. Nikitczuk, B. Weinberg, P. Canavan and C. Mavroidis, Active knee rehabilitation orthotic device with variable damping characteristics implemented via an electrorheological fluid, *IEEE/ASME Transactions on Mechatronics* **15** (2010), 952-960.

[10] Y. Urakami, T. Aoyama, H. Anzai and Y. Kakinuma, Development of tactile display

device using ERG multiple-disk clutch, *Journal of Intelligent Material Systems and Structures* **22** (2011), 1693-1698.

[11] M. Haraguchi, J. Furusho and R. Kawatani, 2-D force display system with redundant ER fluid brake aimed at rehabilitation support system for upper limbs, *Journal of Robotics and Mechatronics* **24** (2012), 731-742.

[12] T. Sun, X. Peng, J. Li and C. Feng, Testing device and experimental investigation to influencing factors of Magnetorheological fluid, *International Journal of Applied Electromagnetics and Mechanics* **43** (2013), 283-292.

[13] V. Trivedi, *Smart actuators for rehabilitation training systems*, MSc. Thesis, University of Dundee, 2009.

[14] D. Senkal and H. Gurocak. Spherical brake with MR fluid as multi degree of freedom actuator for haptics, *Journal of Intelligent Material Systems and Structures* **20** (2009), 2149-2160.

[15] Y. H. Hwang, S. R. Kang, S. W. Cha and S. B. Choi, An electrorheological spherical joint actuator for a haptic master with application to robot-assisted cutting surgery, *Sensors & Actuators, A- Physical* **249** (2016), 163-171.

[16] K. N. An, L. J. Askew and E. Y. Chao, Biomechanics and functional assessment of upper extremities", *Trends in Ergonomics/Human Factors III*, Elsevier Science Publishers, B.V., North-Holland (1986), 573-580.

[17] C. R. Dickerson, B. J. Martin and D. B. Chaffin, The relationship between shoulder torques and the perception of muscular effort in loaded reaches, *Ergonomics* **49** (2006), 1036–1051.

[18] A. Abood, S. Jaffar and M. Qusay, Biomechanical aspects of shoulder and hip articulations: a comparison of two ball and socket joints", *Al-Khwarizmi Engineering Journal* **2** (2005), 61–72.

[19] H. Zhou, M. Bai, Y. He and S. Ren, FEM analysis of magnetorheological fluid seal of circular cooler and its experimental research", *International Journal of Applied Electromagnetics and Mechanics* **41** (2013) 419-431.

[20] LORD MR Fluids Technical Summary, Lord Corporation, www.lordfulfillment.com.

[21] I. H. Shames and F. A. Cozzarelli, Elastic and inelastic stress analysis, Englewood Cliffs, NJ: Prentice-Hall (1992).

[22] A. Almazroa, *Smart actuators and their application to rehabilitation training systems*, MPhil Thesis, University of Dundee, 2011.

[23] A. K. El Wahed and C. A McEwan, Design and performance evaluation of magnetorheological fluids under single and mixed modes, *Journal of Intelligent Material Systems and Structures* **22** (2011), 631-643.

[24] A. K. El Wahed and L. B. Balkhoyor, Magnetorheological fluids subjected to tension, compression, and oscillatory squeeze input, *International and Systems* **16** (2015), 961-980.

[25] A. K. El Wahed and L. B. Balkhoyor, Characteristics of magnetorheological fluids under single and mixed modes, *Proc IMechE Part C: J. Mechanical Engineering Science* **231** (2016), 3798-3809.

[26] MR Fluid MRF-241ES Product Bulletin, Lord Corporation, www.lordfulfillment.com.

[27] D. Guth, M. Aust and J. Maas, Novel concepts for MRF based clutch systems with integrative functionalities, *IEEE/ASME International Conference on Advanced Intelligent Mechatronics*, Montreal, Canada, July 6-9, 2010.

[28] G. Hu, M. Long, L. Yu and W. Li, Design and performance evaluation of a novel magnetorheological valve with a tunable resistance gap, *Smart Materials and Structures*, **23** (2014), Article number 127001.

[29] I. Yazid, S. Mazlan, T. Kikuchi, H. Zamzuri and F. Imaduddin, Design of magnetorheological damper with a combination of shear and squeeze modes, *Materials and Design* **54** (2014), 87–95.

[30] B. Ichwan, S. Mazlan, F. Imaduddin, K. T. Ubaidillahd and M. Idris, Development of a modular MR valve using meandering flow path structure, *Smart Materials and Structures*, **25** (2016), Article number 037001.

[31] ANSYS Technical Team, 2015, Private Communication.

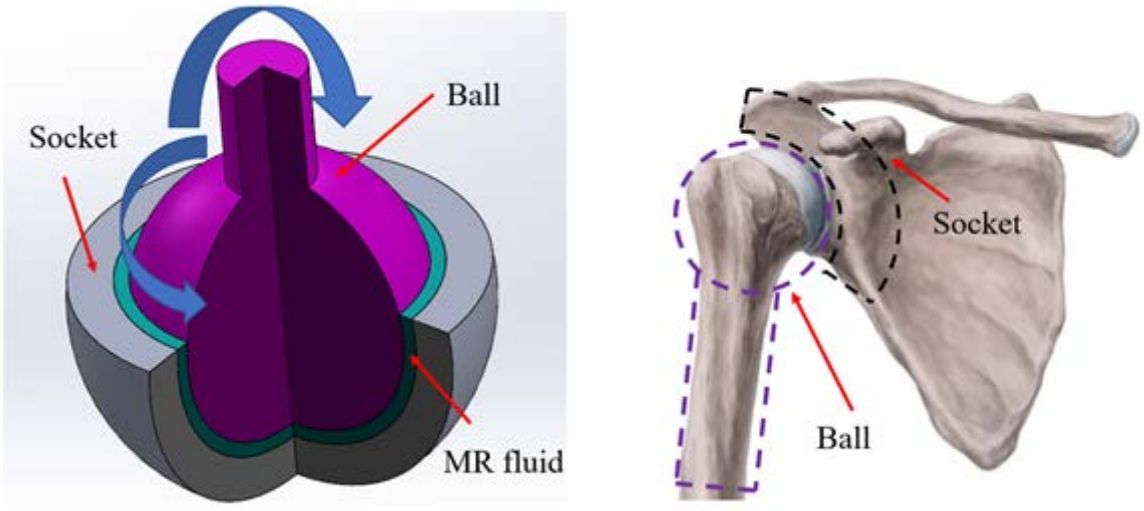

(a) (b)

Fig. 1 Conceptual design of the ball-and-socket actuator: (a) mechanical joint and (b) human shoulder joint.

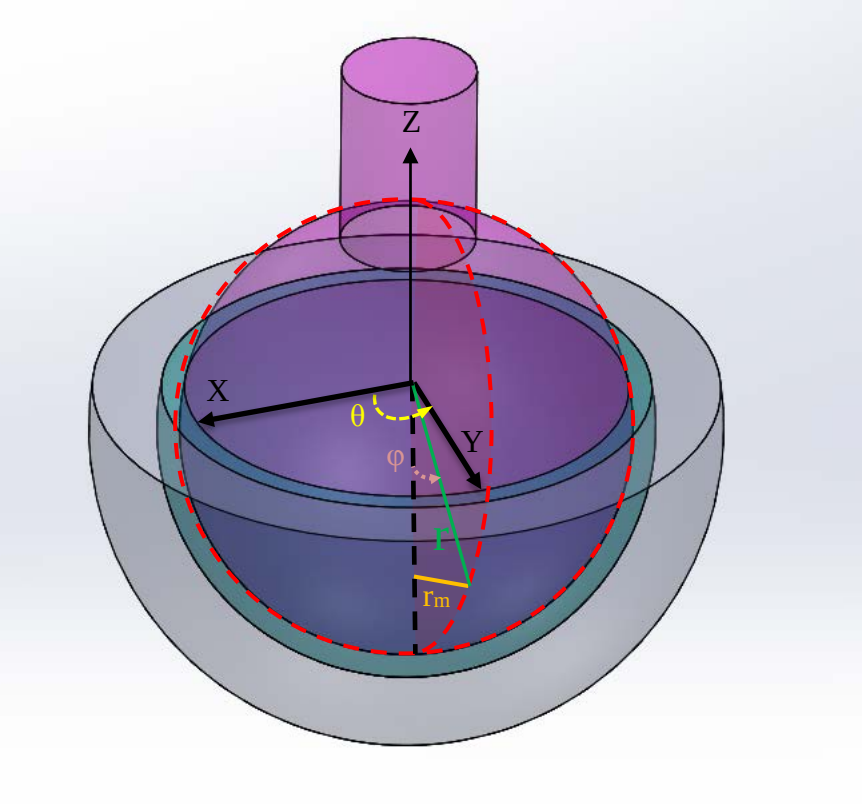

Fig. 2 Schematic diagram showing the spherical coordinate system.

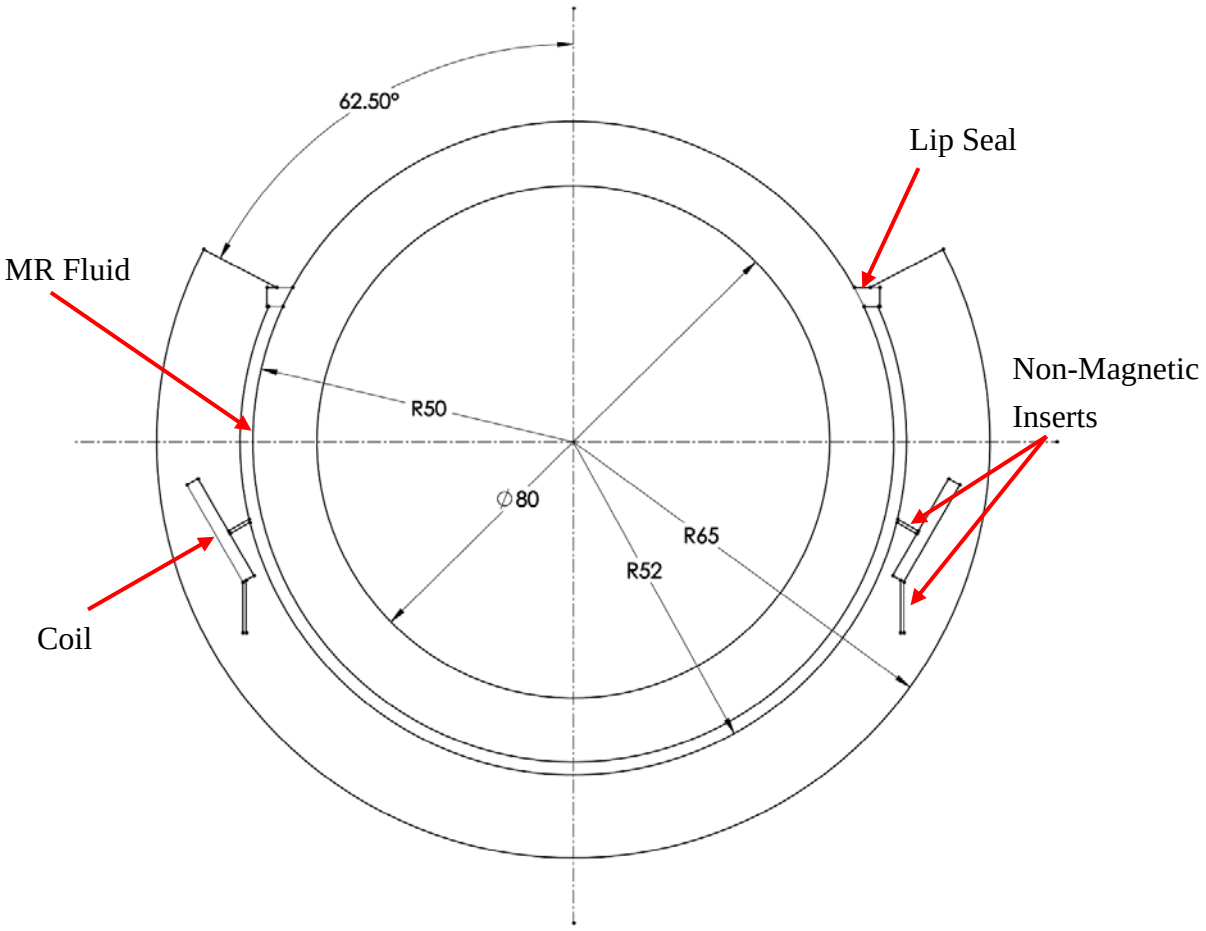

Fig. 3 Geometry of the ball-and-socket actuator with its optimum electromagnetic circuit.

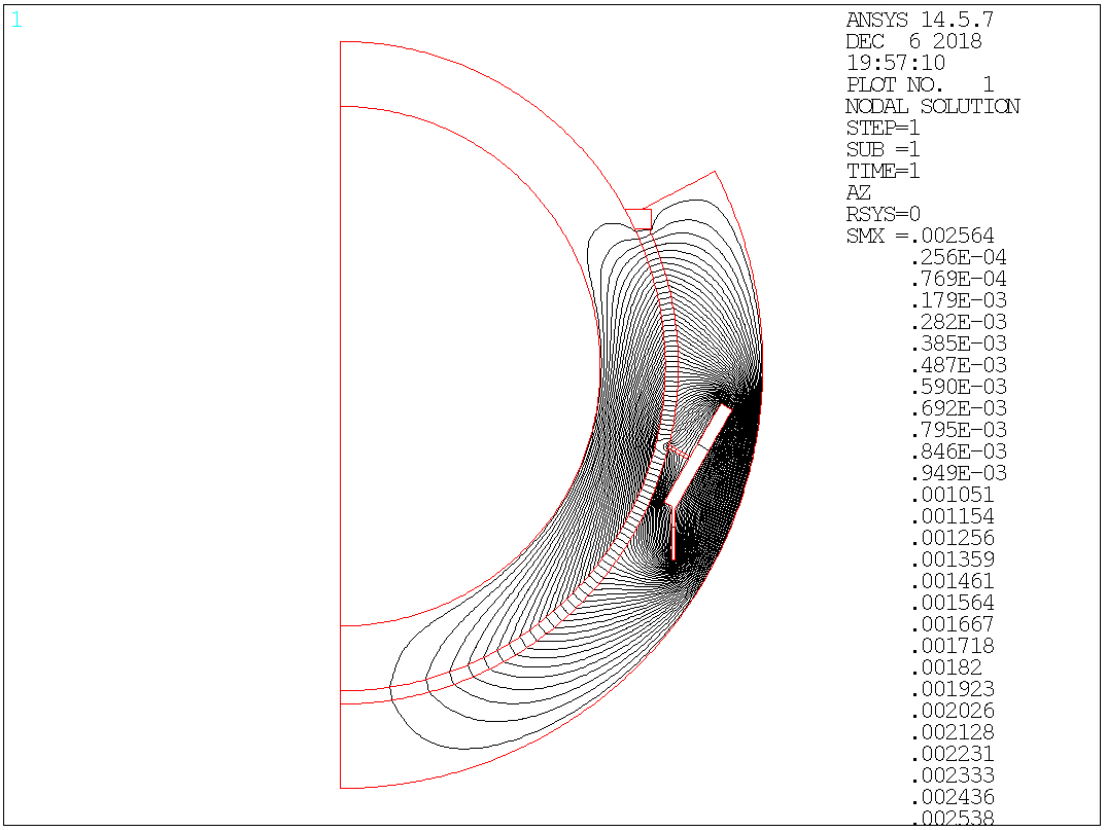

Fig. 4 Half-section view of the ball-and-socket actuator showing magnetic flux distribution across the MR fluid gap.

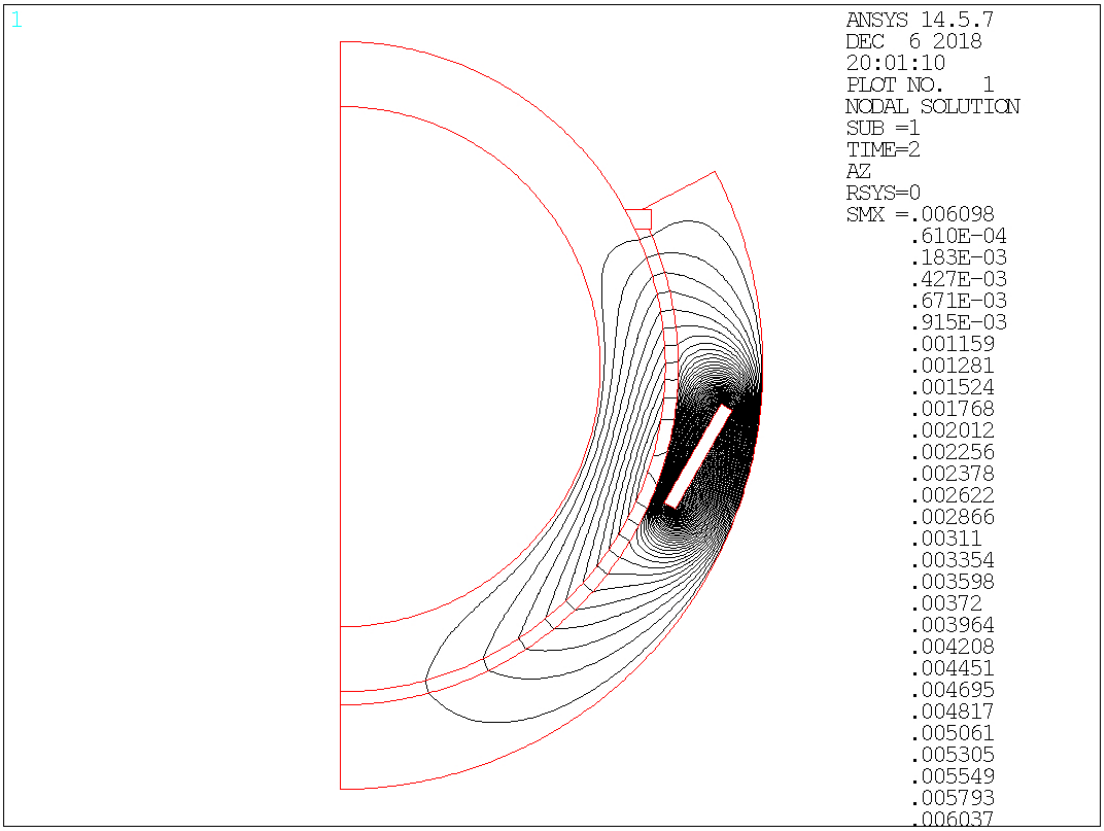

Fig. 5 Impacts on the magnetic flux distribution across the MR fluid gap in the absence of the non-magnetic inserts.

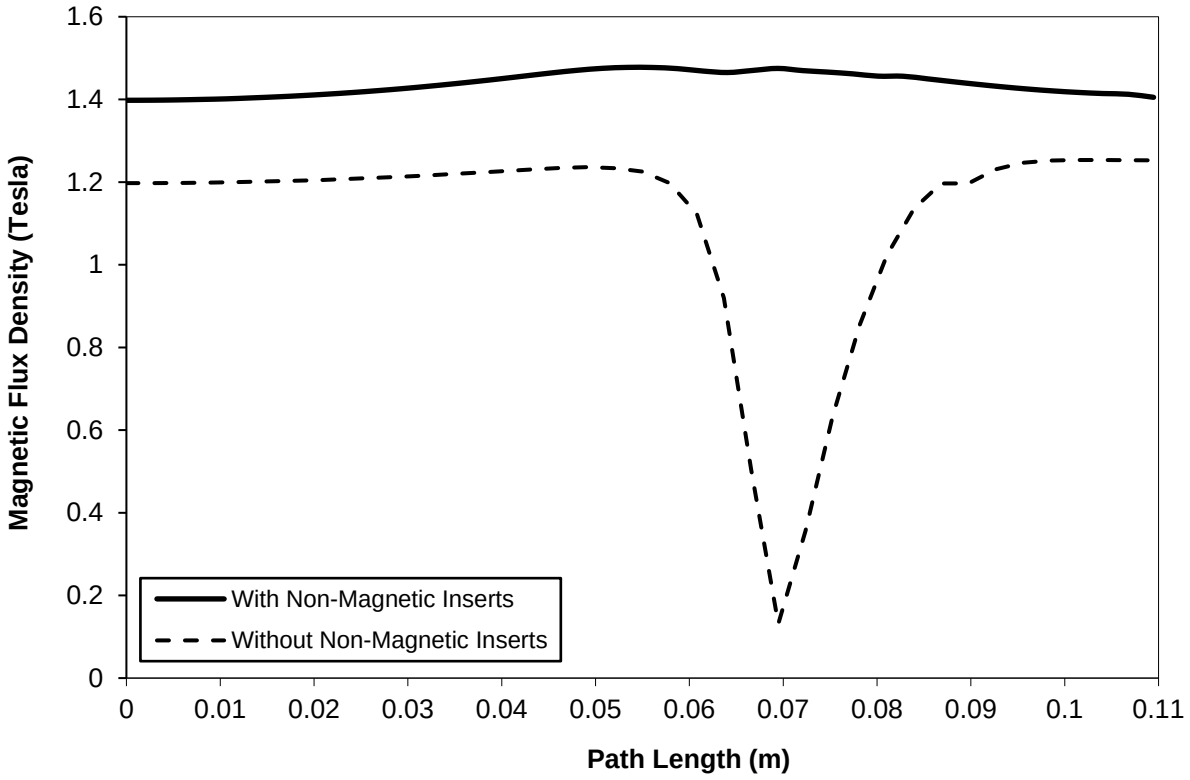

Fig. 6 Magnetic field density variation along half of the median path inside MR fluid gap for the two cases, with and without non-magnetic inserts.

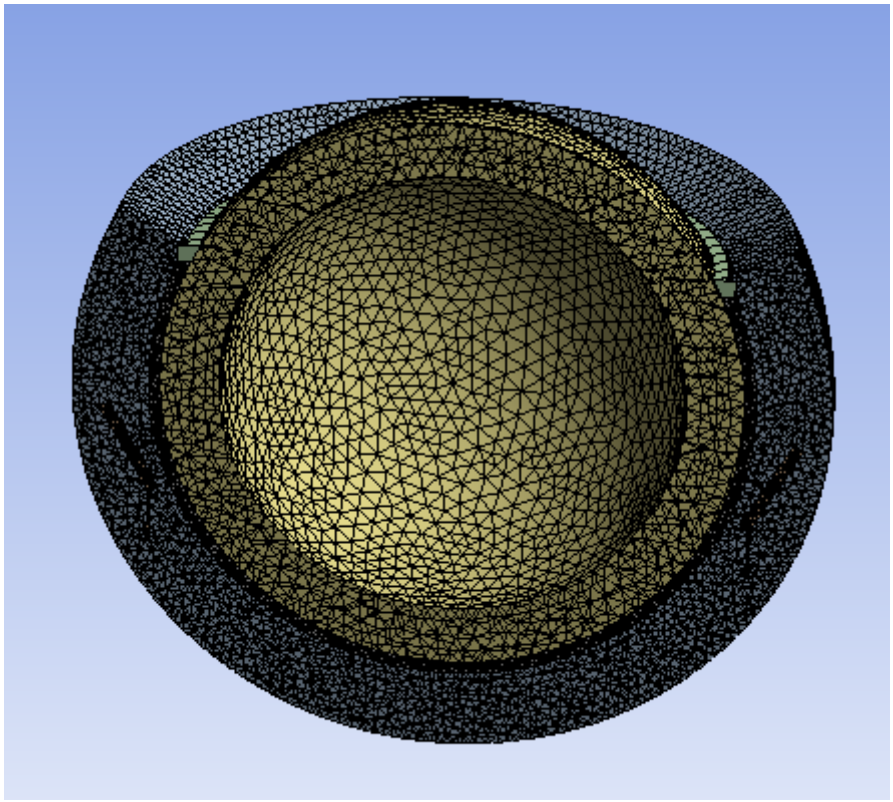

Fig. 7. Meshed model of the ball-and-socket actuator.

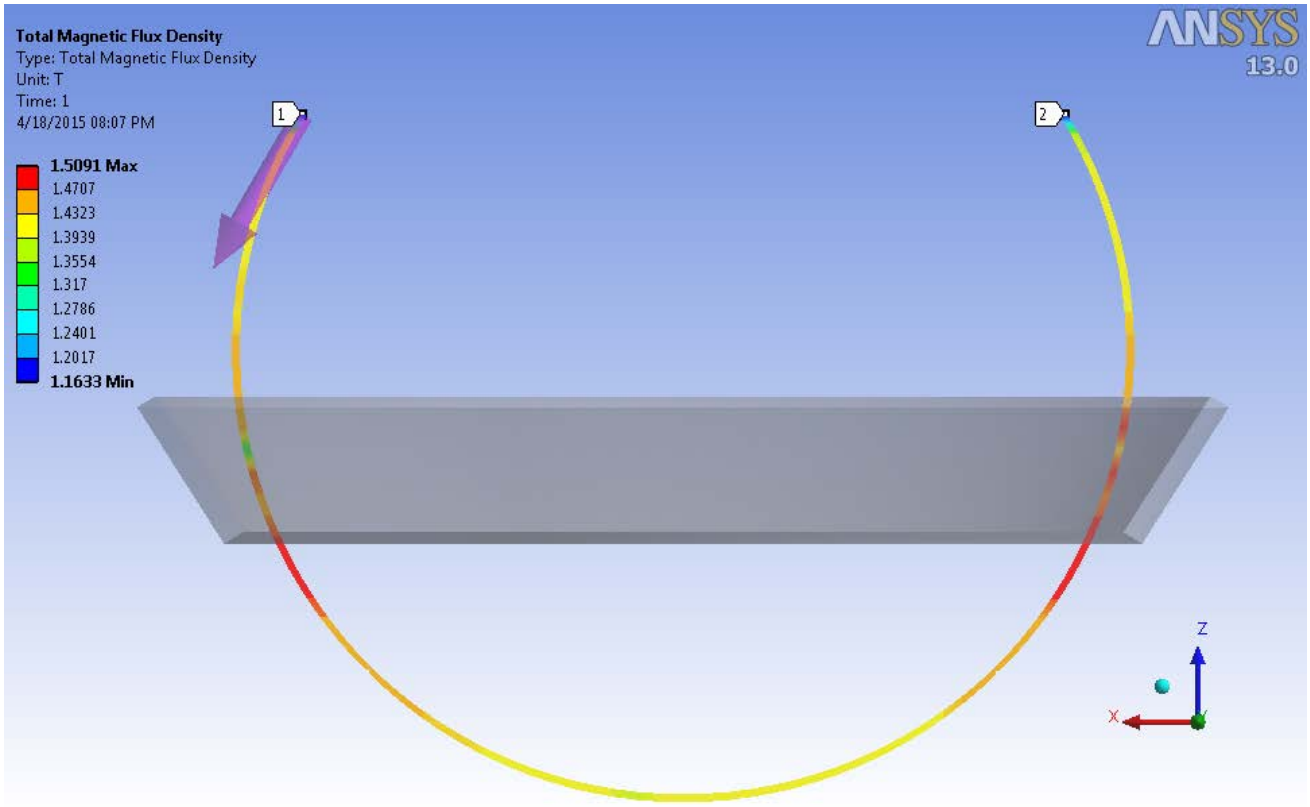

Fig. 8 Magnetic field density distribution along the imaginary median path inside the MR fluid gap of the ball-and-socket actuator.

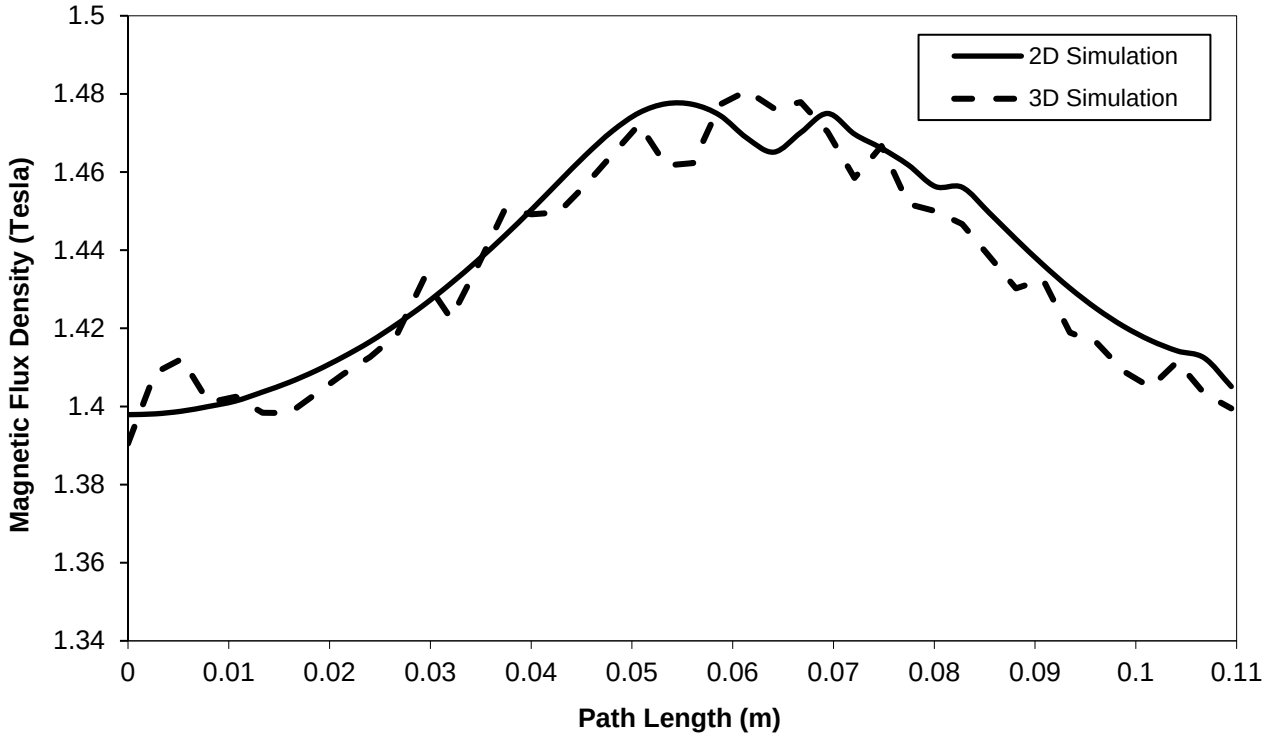

Fig. 9 Comparison of the magnetic field density along the imaginary median path inside the MR fluid gap obtained using 2-D and 3-D ANSYS simulations.

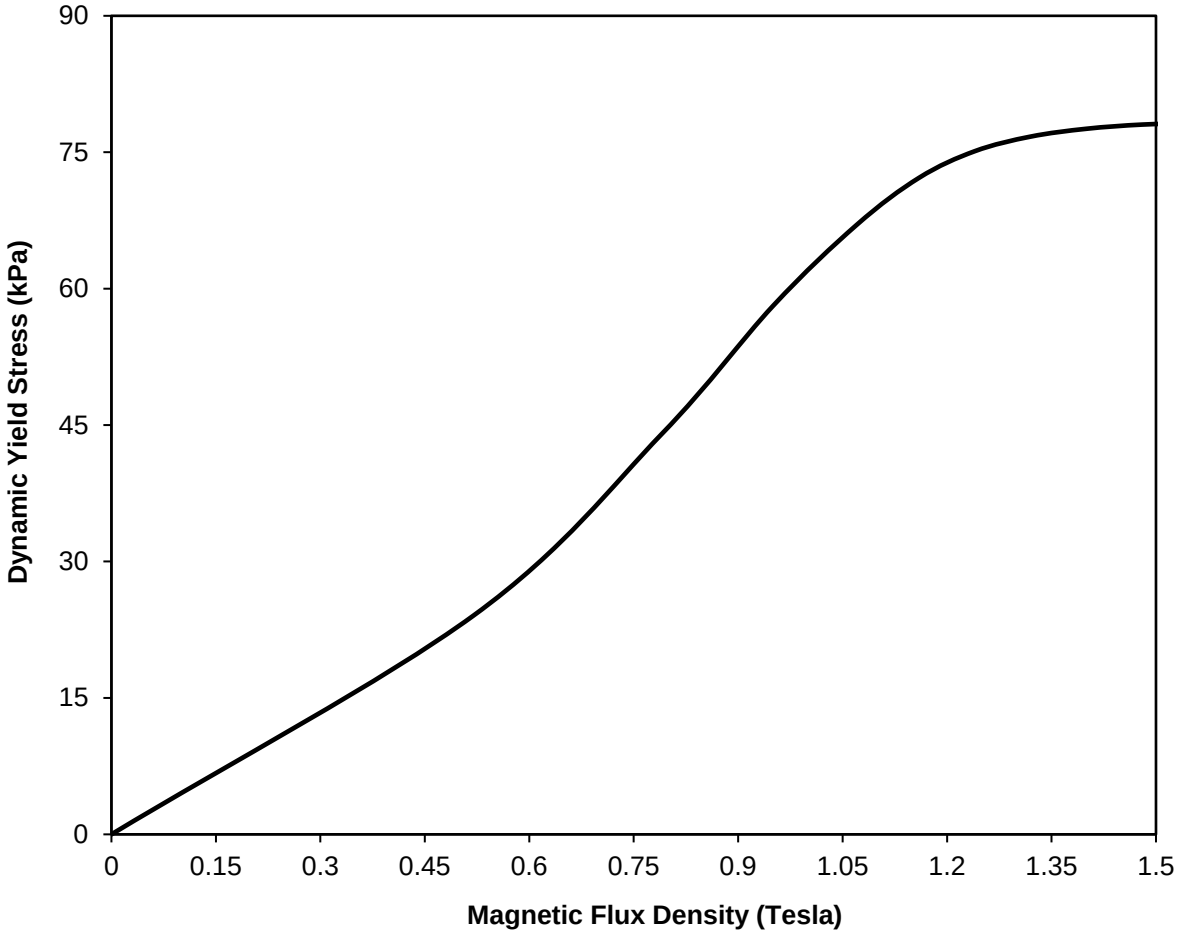

Fig. 10 Dynamic yield stress versus field density for MR fluid MRF241-ES.

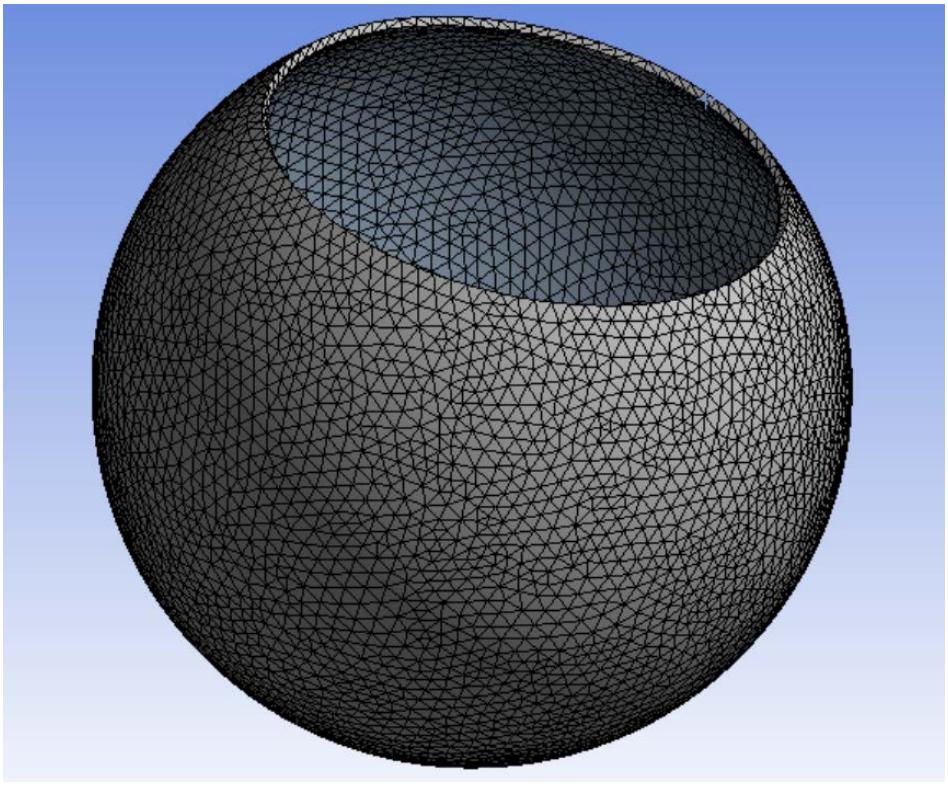

Fig. 11 Meshed MR fluid volume model.

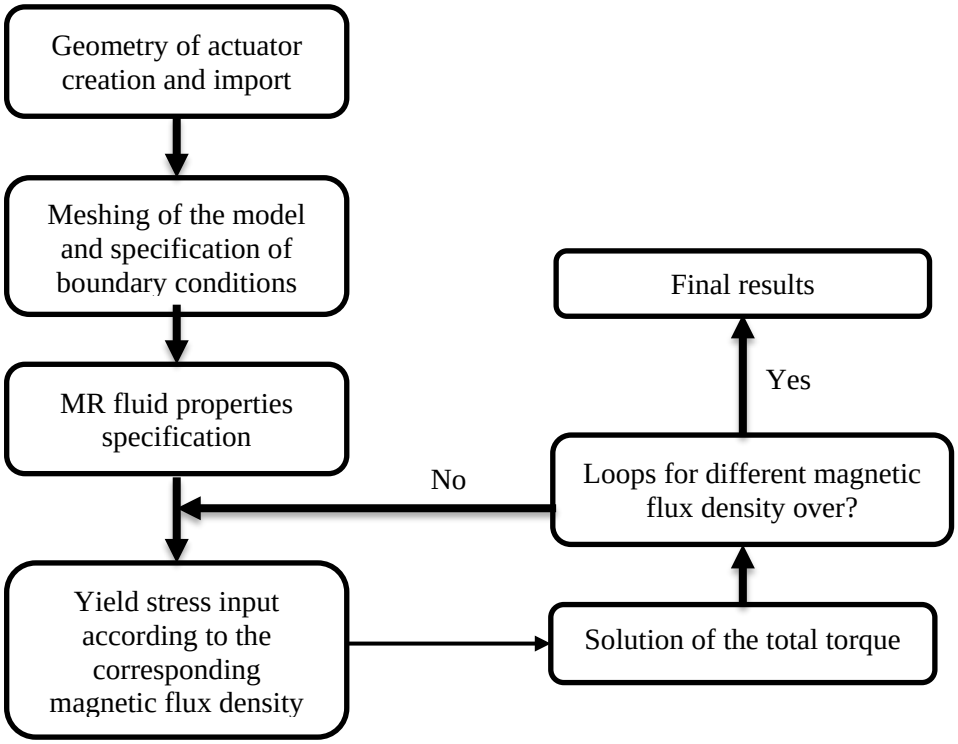

Fig. 12 Flow chart of the CFD simulation procedure.

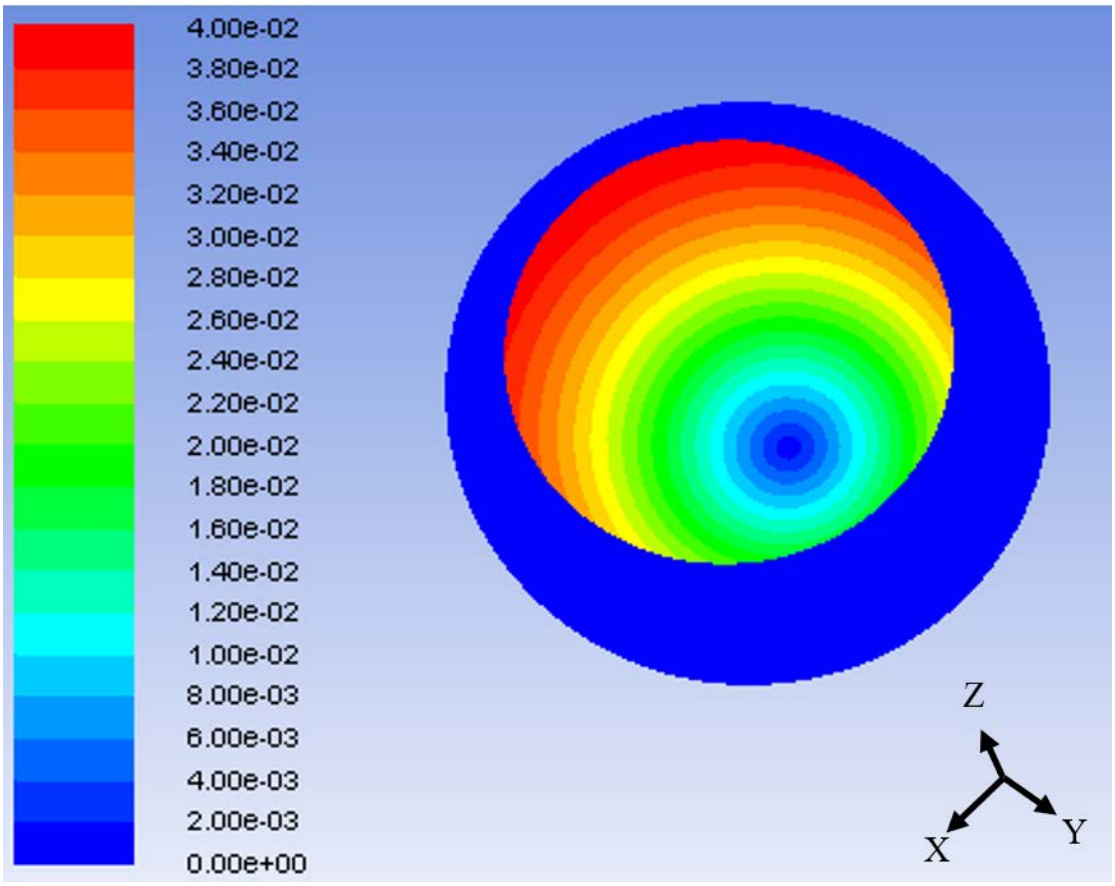

Fig. 13 Isometric view of the velocity contour along the MR fluid volume under a magnetic field density of 0.75 Tesla.

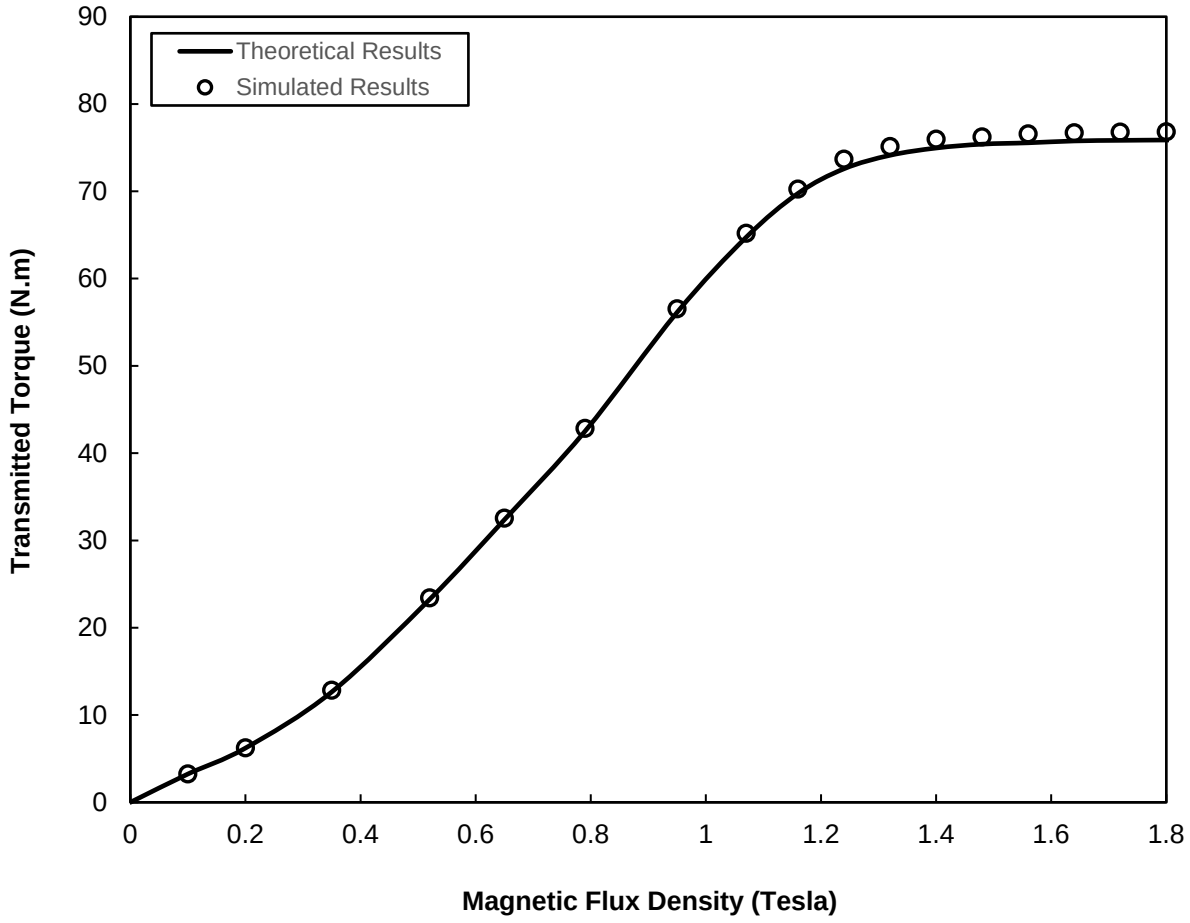

Fig. 14 Transmitted torque versus magnetic flux density.